Determination of surface formation energies on curved single crystals from STM images

Piñeiros Bastidas, J.M.

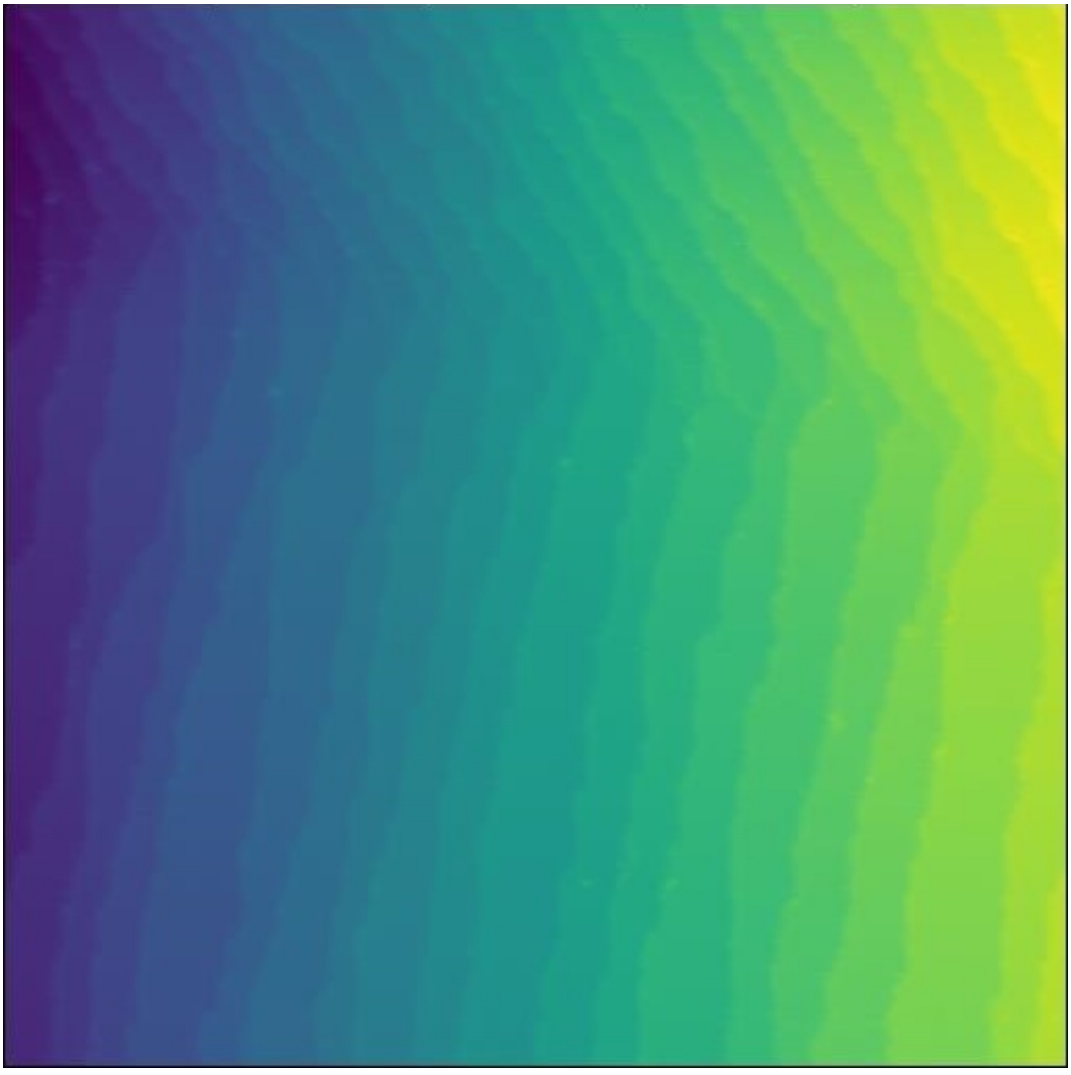

Chapter 4

Straight sections of step edges on a NiAl(110) curved single crystal surface used to calculate an approximation of step formation energy

Curved crystals may feature a smooth transition between different vicinal surfaces. Using one curved single crystal to study different vicinal surfaces requires less experimental time than using several single flat crystals. Here, we study step distributions on the (110) plane of a curved NiAl single-crystal surface, which consists of alternating Ni and Al atom rows. We use scanning tunneling microscopy under UHV conditions at room temperature and our home-built Python-based analysis script to obtain statistical information on kink and straight sections along step edge distributions from STM images. We perform this analysis mainly to study this single crystal's kink distributions and step termination. We propose a new method to estimate the step formation energy based on step edge analysis and statistical mechanics. With this method, we find an approximation of the step formation energy for NiAl(110).

This chapter is based on the following publication:

J. M. Piñeiros-Bastidas, S. V. Auras, L. B. F. Juurlink. "Straight sections of step edges on a NiAl(110) curved single crystal surface used to calculate an approximation of step formation energy". *Surface Science*, vol 749 ,2024.

4.1 Introduction

NiAl is an intermetallic compound broadly used for catalysis and research. The NiAl(110) crystal plane is formed by consecutive rows of Ni atoms and Al atoms. Steps on the NiAl(110) surface are expected to run predominantly along the [001] direction. The NiAl(110) crystal plane has been extensively used to create an Al_2O_3 overlayer (1). Hence, several previous studies regarding surface analysis and oxidation on NiAl exist.

Regarding the surface structure of NiAl, Davis et al., (2) found from LEED (Low energy electron diffraction) analysis, a rippled relaxation on NiAl(110), with Al rows displaced approximately 0.22 Å above the Ni rows. Mullins and Overbury (3) using LEIS (Low-energy ion scattering spectroscopy) analysis, confirmed an Al rippled relaxation on the NiAl(110) surface of 0.21 ± 0.05 Å, and additionally found that the top layer of a NiAl(100) surface contains a significantly larger fraction of Al atoms than Ni atoms. The latter results might be relevant for our analysis because the NiAl(110) steps run along the [001] direction.

Considering the interaction of NiAl with oxygen, NiAl oxidizes easily, forming a thin Al_2O_3 layer (4). Isern and Castro (5) found from Auger studies that after exposure to oxygen, Ni is left unaffected, showing no evidence of a Ni-O interaction. In contrast, Al transforms to the oxide Al_2O_3. During the oxidation of NiAl(110), Jaeger et al., (1) did not find information supporting the formation of Ni-O compounds, such as NiO, $NiAl_2O_4$, nor elemental Ni at the interface Al_2O_3-NiAl.

Another interesting feature of the oxidation of NiAl(110) is that Ni atoms dissolve into the NiAl bulk during the annealing process following surface oxidation, as reported by Jaeger et al., (1). In addition, Lozovoi et al., (6) reported from DFT calculations that during oxidation of NiAl (110), the system dislodges Ni atoms from the surface either by exchanging positions with Al atoms from a sublayer or by filling Ni vacancies in the bulk.

Additionally, defects in the thin oxide overlayer occur and are primarily oriented along the Ni and Al rows and likely originate from monoatomic steps in the NiAl(110) plane (7). In agreement with this article, Pierce et al., (8) observed that oxide rods run along the substrate [001] direction during the initial oxidation of a NiAl(110) surface. These oxide rods can climb or descend to the next substrate terrace by adding or removing atomic layers. Thus, from a practical point of view, this adds another reason to study this system. If oxidation is initiated at steps, control over the defect density in the Al_2O_3 overlayer may be achieved by studying and predicting steps behavior and distribution in

this surface.

Currently, it is unknown whether the steps along the [001] direction on a NiAl(110) surface consist predominantly of Ni or Al. From the studies discussed previously, an Al step termination might be expected on a NiAl (110) crystal surface. Here, as part of our analysis in step termination on NiAl(110), we perform further analysis on STM images, focusing on kinks and straight section distributions along step edges on this surface. This article includes complementary analysis with respect to our previous study (9) on NiAl(110) step edges.

4.2 Material and methods

The crystal is described using the symbology introduced by Auras and Juurlink (10), as c-NiAl(110)[001] 31°. The apex of the curved surface is the (110) plane. The surface may be viewed as a 31°section of a [001] oriented cylinder. The polished area of the crystal is 8 mm long and 7 mm wide. Both sides of the crystal have the same step type. The crystal surface is cleaned with sputtering and annealing cycles. Ar^+ sputtering (0.7 kV, 2.6 µA, 30 min, under a 45° angle from the apex toward [001]) followed by *in vacuo* annealing (950 K, 5 min).

STM images were taken at room temperature in a UHV VT-STM from Omicron. We use the same images analyzed previously (9) for analysis purposes. We analyze quantitatively those images with a home-built Python script (11). Height is defined as the z direction. The y direction runs parallel to the steps, and x runs perpendicular to the steps. Distances along x, i.e., the distance between consecutive atom rows in the (110) plane, and along y, i.e., the distance between two consecutive Ni atoms, or two consecutive Al atoms, along a straight section on a step edge, are scaled to atomic units (a.u.). Atomic units along x are $\sim$ 2.04 Å, and $\sim$ 2.89 Å along y. Schematic representations of the NiAl (110) plane and of a small section of a NiAl(110) surface have been included in reference (9) as Figures 1a and 1b.

We analyze sixteen STM images taken at different positions along the curved surface. These sixteen STM images are included in Appendix B. We use the 2D coordinates of the periodic atomic grid specific to this crystal to analyze step edge distribution. We analyze individual step edges of every STM image independently. The bin size used to create a kink length histogram is the atomic unit along x, i.e., $\sim$ 2.04 Å. The bin size used to create straight sections length histograms is the atomic unit along y, i.e., $\sim$ 2.89 Å. Even

though the bin sizes on kinks and straight sections histograms are numerically different, we keep the notation as (a.u.) because they both represent distances between consecutive atoms.

4.3 Results

Before describing the analysis of step distributions on NiAl(110), we show a 3D plot of the surface of one of the images analyzed, image B.S1g (Appendix B). The 3D plot shown in Figure 4.1a depicts terrace coordinates in cyan plotted over the raw data in red. We can see the variation in terrace width within the image. This plot represents an image taken on the left side of the crystal; as such, it steps down from right to left. We highlight the step edges coordinates in purple.

NiAl(110) terraces with steps running along the [001] direction step down from one atom type to the same atom type, i.e., if the step edge of one terrace terminates in Ni atoms, the next consecutive terrace will start with Ni atoms. If, for example, we consider the first step edge on the right of Figure 4.1a as step edge ♯1, the next step edge to the left is step edge ♯2, and so on. Since terraces step down from one atom type to the same atom type, we need to displace all the odd step edge numbers by one atomic unit for the analysis with the crystal's 2D atomic grid. There is no need to displace even step edges because, following this principle, they should be displaced two times, which implies that the step edge remains in the same atom type as originally.

We use these displaced step edge coordinates to generate the 'grid-fitted' step edges by comparing the coordinates of every step with the coordinates of the atomic grid and selecting the closest atomic grid position to each step edge coordinate. Figure 4.1b illustrates small sections of the top view of two consecutive step edges as red lines superimposed on the atomic grid. The purple and green circles represent consecutive Ni and Al atom rows. This plot includes straight sections and kinks along step edges. We use the data of the 'grid-fitted' step edges to analyze and quantify kinks and straight sections on step edges.

For the kink analysis, we use kinks that occur in the expected geometry, i.e., the expected angle. Several kinks of single, double, and triple lengths are visible in Figure 4.1b. In Figure 4.1c, we show a kink length histogram for ten high-resolution images, with sizes ranging from 50 nm x 50 nm to 200 nm x 200 nm. The plot shows the normalized occurrence of kinks versus their length in atomic units along x. Monoatomic kinks occurred in more than 80%

Straight sections of step edges on a NiAl(110) curved single crystal surface used to calculate an approximation of step formation energy

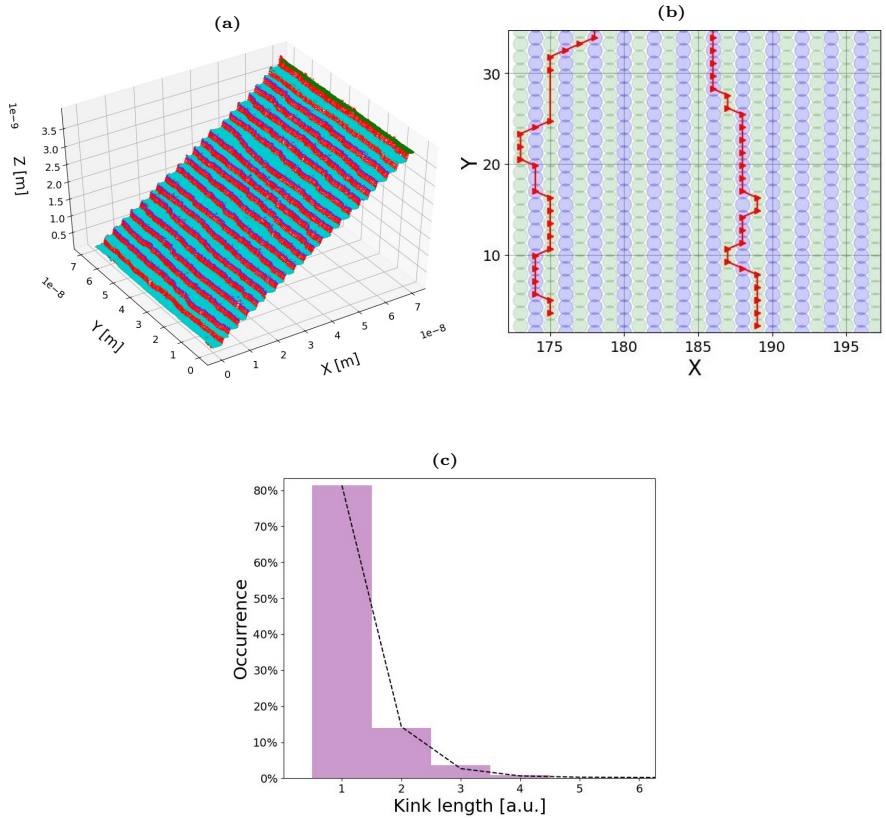

Fig. 4.1: a) 3D plot of a NiAl(110) crystal surface with terraces and step edges highlighted in cyan and purple, respectively. b) The top view of small sections of two consecutive step edges is shown as red lines superimposed on the atomic grid. The purple and green circles represent the atomic grid (xy plane) of NiAl (110) terraces. c) Normalized occurrence of kink lengths for ten high-resolution images. Kink lengths are measured in atomic units (a.u.) along the x direction. An exponential approximation is included as a black dashed line.

of the cases; diatomic kinks in $\sim$ 15%, and triatomic kinks in less than 5%. The preferred occurrence of monoatomic kinks requires regular switching of termination of terraces by Ni to Al or vice versa.

In the kink length histogram shown in Figure 4.1c, we observe a steep decay that resembles an exponential decay. We calculate an exponential fit of the kink length histogram and include it as a black dashed line. The exponential fit used is equation 4.1, with *a, b* and *c* constants and x the variable. The parameters of this free fit are $a = 4.668$, $b = 1.750$,$c = 0.002$, and the variable is the kink length in atomic units along the x direction.

$$y = ae^{-bx} + c \tag{4.1}$$

The difference between the kink quantification shown in this article with respect to our previous study (9), is the number of images used for the analysis. Instead of three images with the highest resolution, we now use ten high-resolution images. The results are very similar, indicating that monoatomic kinks are favored. Step edges must, therefore, alternate between Ni and Al atom rows. This analysis, however, does not imply a potential preference in step termination by Ni or Al.

To gather more information, we also analyze the straight sections in all the steps. We start by numbering the first atom row along y on the left of the atomic grid as ♯1 and the consecutive rows as rows ♯2, ♯3, and so on. Once we have distinguished even from odd y atom rows, we measure the length of every straight section along each step edge in an STM image in atomic units (a.u.). We do this for ten high-resolution images.

Before attempting to identify a preferred terrace termination by Ni or Al, we must consider the following two points. Firstly, the assignment of atom row numbers cannot be connected directly to atom types. Even and odd atom rows may be associated with either Ni or Al for each STM image. Secondly, as previously discussed (9), large STM images have intrinsically low spatial resolution. For example, one of our images contains 0.1499 pixels/a.u., which is in excellent agreement with the expected scaled value of 0.1495 pixels/a.u. (See Appendix B for details). However, the difference of 0.0004 pixel/a.u. between the expected scaled value and the observed histogram's bins frequency results in an uncertainty of 0.3% along x, representing three pixels per a thousand (a.u.), or equivalently one pixel every 333.33 (a.u.). This difference results in an identity switch of even and odd row numbers concerning them representing Ni or Al every 333.33 (a.u.) along x. We cannot tell, however, where in the

STM images this switch occurs as they have been cropped, e.g., to remove partial steps occurring at the edges of the STM images.

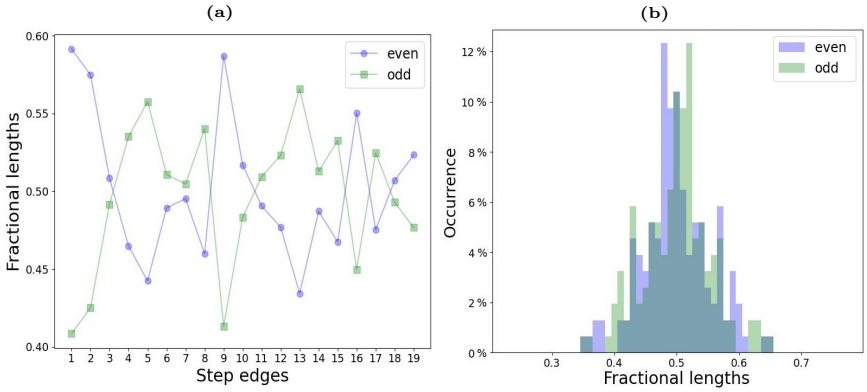

Fig. 4.2: a) Fractional lengths of even and odd straight sections plotted for nineteen step edges in image B.S1d (Appendix B). b) Normalized occurrence of even and odd fractional lengths for ten high-resolution images together, including the data from a).

Regardless of these two uncertainties, we can use the distribution of straight lengths to come to a conclusion regarding a potential preference to terminate terraces with either Ni or Al. If one element is preferred to terminate a terrace, we should find slightly more of this element type at every step. The fractional occurrence of straight lengths in the even vs. odd y atom rows should then deviate from a 50-50 distribution. For example, if Ni terminates terraces on average 60% of the time and Al 40%, we would find a ratio on the order of 60-40 when summing the straight sections along the even and odd y atom rows for a single step. We are unlikely to find exactly 60-40, as some statistical distribution around these mean values for Ni and Al must occur when analyzing a single step of limited length. If we include the fractional lengths of many steps from multiple images, we would still find a bimodal distribution with one mode centered around 60% and another centered around 40%. This holds true regardless of the two discussed uncertainties unless the two distributions are so closely spaced and/or very broad that they appear as a single, broad distribution.

Figure 4.2a shows the fractional lengths in even and odd y atom rows (purple and green) for a single image, B.S1d (Appendix B), containing nineteen

steps. We calculate the fractional length in each step by summing the straight sections along y for even and odd atom rows separately and dividing those values by the total straight length of the step. Clearly, the data for a single color (atom type) varies from left to right in the image but without a clear pattern. The fractional length oscillates mostly between ~ 0.4 and ~ 0.6, but most step edges remain close to 0.5. We note that the irregular oscillation can not be ascribed to identity switching as resulting from the minor uncertainty along x (see above). Based on the size of this STM image, an identity switch could have happened only once in this Figure. We find the same behavior of irregular variations in the fractional occurrences between consecutive steps in all of the ten high-resolution STM images, as shown in Figure 4.2b.

To check for a potential bimodal distribution, we have added the data from all nineteen steps in Figure 4.2a and then added the same type of data for another nine high-resolution images. The normalized occurrence as a function of fractional lengths is shown for even and odd y atom rows, binned with a bin width of 0.01, and maintaining the color coding. We fit both histograms with a Gaussian line shape. The standard deviation for the even and odd distributions is exactly the same, 0.0546, and the mean values are 0.499 and 0.501, respectively. The distributions are, thus, virtually identical and well-described by a single Gaussian line shape. There is no reason to assume a bimodal distribution with these narrow widths and virtually identical mean values. Hence, our statistical analysis of the occurrence of straight sections in the even and odd y atoms rows points toward no preference for Ni vs Al terrace termination.

To further investigate a possible difference between terrace termination by Ni and Al, we analyze the length distribution of straight sections in even and odd y atom rows. For instance, Figure 4.3a includes a straight section length histogram for one image with high resolution, B.S1j (Appendix B), as normalized occurrence vs atomic units in even and odd y atom rows.

Here, the difference in normalized occurrence per bin in straight section length ranges between $\sim 1\%$ and $\sim 2\%$ for even and odd y atom rows. Although we cannot distinguish between the two atom types, the histogram indicates that Ni and Al terrace termination is characterized by the same straight length distribution.

The difference in normalized occurrence per bin between even and odd y atom rows remains around $\sim 2\%$ or below for the ten high-resolution images. Thus, we add the data from even and odd straight sections. The difference between even and odd normalized occurrences with respect to the data added together per bin is smaller than $\sim 0.26\%$. We conclude that summing data from

various edges or multiple images does not affect the analysis and conclusions on straight length distributions. Again, we find no statistical difference, hence no evidence of a preference for either Ni vs Al terrace termination.

The straight section length histogram for ten high-resolution images is plotted in Figure 4.3b, which includes data from 14817 straight sections. The majority of the data of this histogram is represented between 1 and 9 (a.u.). Data from 10 (a.u.) upward has less than $\sim 1\%$ of occurrence. Monoatomic straight sections occurred in $\sim 37\%$ of the cases, while diatomic and triatomic straight sections occurred in $\sim 20\%$ and $\sim 12\%$, respectively. This histogram shows an exponential decay. We calculate an exponential fit of the straight section length histogram using equation 4.1 and plot it as a black dashed line. The parameters of this free fit are $a = 0.574$, $b = 0.491$,$c = 0.003$, and the variable is the straight section length in atomic units along the y direction. The high occurrence of short straight sections indicates the meandering of the step edge. We find a few long, straight sections in some images, representing only a small fraction of the occurrence.

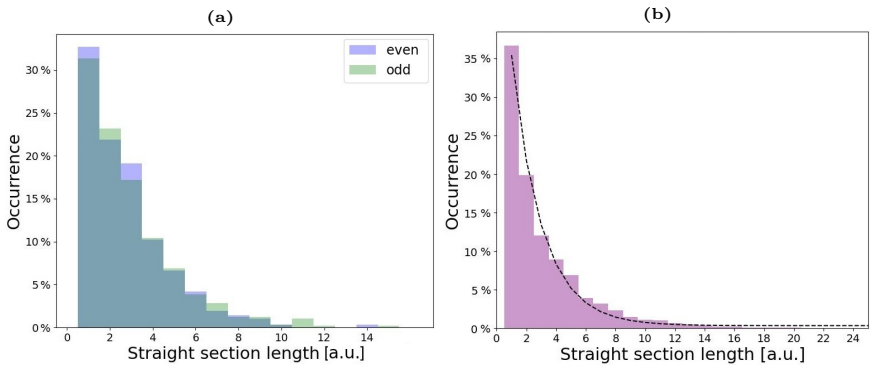

Fig. 4.3: a) Normalized occurrence of even and odd straight section lengths for the high-resolution STM image B.S1j (Appendix B). Straight sections are measured in atomic units (a.u.) along the y direction. b) Normalized occurrence of straight section lengths for ten high-resolution images together. Straight sections are measured in atomic units (a.u.) along the y direction. An exponential approximation is included as a black dashed line.

Since all data analysis is consistent with no significant preference in steps terminating in Ni or Al, we now visualize the step edge as a string of atoms that, with each next atom, either continue a straight section or introduce a kink. Considering the step termination in this crystal surface as a canonical

ensemble in thermodynamic equilibrium and using statistical mechanics theory, the probabilities of step atoms continuing along straight sections or introducing kinks should follow a Boltzmann distribution (12).

The probabilities of finding a step continuing in straight sections or kinks, P_S, and P_K, respectively, are given by equations 4.2 and 4.3, where η is the step formation energy and ϵ is the kink formation energy. These equations represent the probability that the system occupies two different microstates with energies η and ϵ. As a simplification, the ratio between probabilities P_S and P_K calculated from equations 4.2 and 4.3, is shown in equation 4.4.

$$P_S = \frac{e^{-\eta/k_BT}}{e^{-\eta/k_BT} + e^{-\epsilon/k_BT}} \tag{4.2}$$

$$P_K = \frac{e^{-\epsilon/k_BT}}{e^{-\eta/k_BT} + e^{-\epsilon/k_BT}} \tag{4.3}$$

$$\frac{P_S}{P_K} = \frac{e^{-\eta/k_BT}}{e^{-\epsilon/k_BT}} = e^{-(\eta-\epsilon)/k_BT} \tag{4.4}$$

$$\eta = \epsilon - ln(P_S/P_K).k_bT \tag{4.5}$$

We use the 'grid-fitted' step edges to evaluate probabilities of step edges continuing in straight sections or kinks, P_S and P_K, respectively. These probabilities are determined as the number of favorable outcomes divided by the total number of outcomes, i.e., the total number of atoms in straight sections or kink sections per step edge divided by the total number of atoms along the step. We separately add straight sections and kink sections along step edges per image for the three highest-resolution images. Then, we calculate the ratio P_S/P_K, as the total number of atoms in straight sections divided by the total number of atoms in kink sections per image. Finally, we average the ratio P_S/P_K for those three highest-resolution images and obtain a numerical value of 2.79. From equation 4.4, we can write an expression for the step formation energy, η, as given in 4.5.

Using equation 4.5, the calculated averaged ratio P_S/P_K, and the kink formation energy previously reported in (9), we determine the step formation energy for straight sections, i.e., step formation energy for NiAl(110) at room temperature. With this new method, we find an average value of 31 ± 4.4 meV/a.u. for the subset of the three highest-resolution images.

We found earlier calculations based on the embedded atom method (EAM) of step formation energy for a Ni(110) surface. Values of 10 meV/Å (20.4

meV/a.u.) for the open [110] steps and 54 meV/Å (110.3 meV/a.u.) for the close-packed [001] steps at 0 K were reported (13). We are unaware of energy calculations or measurements on NiAl and provide the value of 31 meV/a.u. as an approximation for a future theoretical study.

We have included a plot of the step formation and kink formation energies as a function of temperature in Figure 4.4a. Step formation energy is calculated with equation 4.5. Kink formation energy calculation is based on the step diffusivity and the mean square displacement of a step position for steps oriented along a high symmetry direction, as previously discussed in (11). Here, we see that creating a kink requires more energy than continuing the step as a straight section, i.e., it is less energetically favorable for the step to meander. A plot of the step formation versus kink formation energy is shown in Figure 4.4b. The slope is 0.54, which indicates that kink formation energy increases slightly faster with temperature than step formation energy.

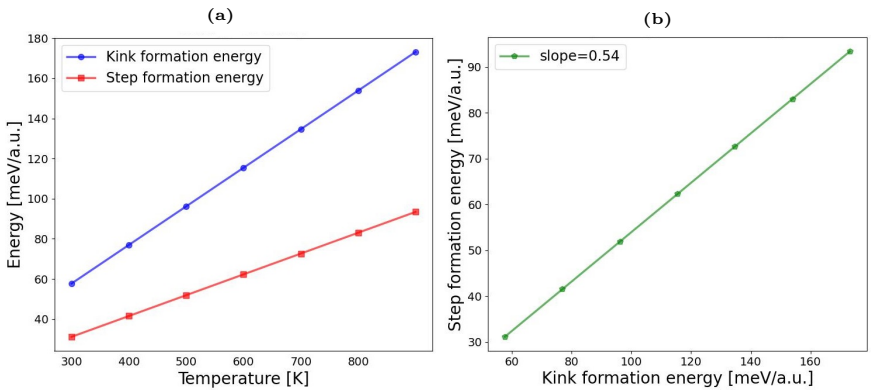

Fig. 4.4: a) Step formation and kink formation energies [meV/a.u.] as a function of temperature [K] for the three highest-resolution images. b) Plot of the step formation versus kink formation energy, [meV/a.u.].

4.4 Conclusion

In this article, we analyzed step edges from STM images in more detail on a curved NiAl(110) single crystal under UHV conditions. We focused on studying the presence of a preferred step termination in our data set.

Similarly to our conclusions from the earlier analysis of kinks (9), we find a preference for monoatomic kinks. This requires that both Ni and Al rows terminate terraces. We quantified the kink length occurrence from ten high-resolution images and found a distribution that an exponential fit can accurately model.

The distribution of straight lengths can also be modeled accurately by an exponential fit. The high occurrence of short straight sections implies significant meandering of step edges, hence a modest difference between step and kink formation energies. No indication of a preferred step termination can be obtained from the straight section length analysis either. Furthermore, the lack of any preference for even or odd straight sections and their identical straight length distributions suggest that Ni and Al both terminate terraces in rather identical manners.

From the distributions of kinks and straight sections along step edges, we see that kinks decay steeper than straight sections decay along step edges. This suggests that after a monoatomic kink, forming a small section along the [111] direction, i.e., creating a diatomic kink, is more energetically costly than starting a new step edge along the [001] direction.

The absence of a preference for Ni or Al to terminate terraces causes step edges to meander considerably on a curved NiAl(110)[001] single crystal. This might constitute one of the reasons why various Al_2O_3 domains occur when oxidizing a NiAl(110) surface. This also limits options for modifying the surface selectively at step edges.

Larger differences between the step and kink formation energy of two elements in a bimetallic substance may allow for chemically-sensitive alteration, e.g., oxidation and pinning, of these edges and control over domain orientation, creation of particular terrace widths or coral-shaped domains with interesting electronic, phononic or catalytic properties.

With our proposed method based on the kink formation energy calculation, probabilities of steps continuing in straight sections or kinks, and statistical mechanics, we find an approximation of the step formation energy for NiAl(110) of 31 ± 4.4 meV/a.u.

Acknowledgement

We are greatly indebted to Prof. Dr. Enrique Ortega for allowing S.A. to collect the used STM images in his laboratory and Max Ilyn for experimental guidance. We also kindly thank Prof. Dr. H. J. W. Zandvliet for useful discussions. The research is funded by STW (now TTW) project #15281 of the Dutch Research Council (NWO).

Bibliography

[1] R. Jaeger, H. Kuhlenbeck, H.-J. Freund, M. Wuttig, W. Hoffmann, R. Franchy, and H. Ibach, "Formation of a well-ordered aluminium oxide overlayer by oxidation of NiAl(110)," *Surface Science*, vol. 259, no. 3, pp. 235 – 252, 1991.

[2] H. L. Davis and J. R. Noonan, "Rippled Relaxation in the (110) Surface of the Ordered Metallic Alloy NiAl," *Phys. Rev. Lett.*, vol. 54, pp. 566–569, 1985.

[3] D. Mullins and S. Overbury, "The structure and composition of the NiAl(110) and NiAl(100) surfaces," *Surface Science*, vol. 199, no. 1, pp. 141 – 153, 1988.

[4] A. Lozovoi, A. Alavi, and M. Finnis, "Surface energy and the early stages of oxidation of NiAl(110)," *Computer Physics Communications*, vol. 137, no. 1, pp. 174 – 194, 2001.

[5] H. Isern and G. Castro, "The initial interaction of oxygen with a NiAl(110) single crystal: A LEED and AES study," *Surface Science*, vol. 211-212, pp. 865 – 871, 1989.

[6] A. Y. Lozovoi, A. Alavi, and M. W. Finnis, "Surface Stoichiometry and the Initial Oxidation of NiAl(110)," *Phys. Rev. Lett.*, vol. 85, pp. 610–613, 2000.

[7] L. Heinke, L. Lichtenstein, G. H. Simon, T. König, M. Heyde, and H.-J. Freund, "Structure and electronic properties of step edges in the aluminum oxide film on NiAl(110)," *Phys. Rev. B*, vol. 82, p. 075430, 2010.

[8] J. P. Pierce and K. F. McCarty, "Self-assembly and dynamics of oxide nanorods on NiAl(110)," *Phys. Rev. B*, vol. 71, p. 125428, 2005.

[9] J. M. Piñeiros-Bastidas, S. V. Auras, and L. B. Juurlink, "A study of step defects on NiAl(110) using a curved single crystal surface," *Surface Science*, vol. 732, p. 122270, 2023.

[10] S. V. Auras and L. B. Juurlink, "Recent advances in the use of curved single crystal surfaces," *Progress in Surface Science*, vol. 96, no. 2, p. 100627, 2021.

[11] J. M. Piñeiros-Bastidas, S. V. Auras, and L. B. Juurlink, "A Python script to automate STM image analysis for stepped surfaces," *Applied Surface Science*, vol. 567, p. 150821, 2021.

[12] C. Kittel and H. Kroemer, *Thermal physics*. 1980.

[13] C.-L. Liu and J. B. Adams, "Step and kink formation energies on fcc metal surfaces," *Surface Science*, vol. 294, no. 3, pp. 211 – 218, 1993.